



# Fast-track preparation of lung specimens for electron microscope observations of the pulmonary endothelial glycocalyx

Mone Wakatsuki<sup>1</sup> · Takashi Takaki<sup>2,4</sup> · Akira Ushiyama<sup>3</sup> · Kazuho Honda<sup>4</sup> · Takehiko Iijima<sup>1</sup>

Received: 21 April 2023 / Accepted: 14 June 2023 / Published online: 5 July 2023  
© The Author(s) under exclusive licence to The Japanese Society for Clinical Molecular Morphology 2023

## Abstract

The glycocalyx (GCX) covers the luminal surface of blood vessels and regulates vascular permeability. As GCX degradation predicts various types of vasculopathy, confirming the presence of this structure is useful for diagnosis. Since the GCX layer is very fragile, careful fixation is necessary to preserve its structure. We explored appropriate and feasible methodologies for visualizing the GCX layer using lung tissue specimens excised from anesthetized mice. Each specimen was degassed and immersed in Alcian blue (ALB) fixative solution, and then observed using electron microscopy. Specimens from septic mice were prepared as negative GCX controls. Using these immersion-fixed specimens, the GCX layer was successfully observed using both transmission and scanning electron microscopy; these observations were similar to those obtained using the conventional method of lanthanum perfusion fixation. Spherical aggregates of GCX were observed in the septic mouse specimens, and the GCX density was lower in the septic specimens than in the non-septic specimens. Of note, the presently reported methodology reduced the specimen preparation time from 6 to 2 days. We, therefore, concluded that our novel method could be applied to human lung specimens and could potentially contribute to the further elucidation of vasculopathies.

**Keywords** Glycocalyx · Immersion fixation · SEM · TEM · Fast-track preparation · Sepsis · Lung tissue

## Introduction

The glycocalyx (GCX) is an endothelial surface layer that covers the luminal surface of arteries, veins, and capillaries. This layer contributes to the efficient transport of plasma and hematopoietic cells and seals the intravascular space [1, 2]. Thus, the destruction of the GCX triggers various modes of vasculopathy, including pulmonary edema and pneumonia [3, 4]. On the other hand, the GCX can be restored concurrently with recovery from sepsis [5]. Thus, the GCX has

been recognized as a putative key factor in the development of organ damage arising from vasculopathy. The lungs contain a vascular architecture that facilitates gas exchange through an ultra-thin membrane. In this architecture, the glycocalyx plays a crucial role in maintaining appropriate fluid transport. Various pathophysiological conditions can damage this barrier, allowing the migration of hematopoietic cells (including macrophages and leukocytes) as part of the infection cascade. The breakdown of the GCX facilitates a proactive immune response, activating residential hematopoietic cells. However, changes to the GCX can also enhance fluid leakage, hindering oxygenation and gas exchange. This pathophysiological process is involved in the development of pulmonary distress. The evaluation of GCX damage could become a significant index for determining the prognosis of patients with pulmonary distress and for evaluating the efficacies of therapeutic interventions. Theoretically, the GCX could be an important component in investigations of the development of pulmonary distress, but damage evaluations are not clinically feasible because of the difficulty in visualizing this component. Alternatively, GCX fragments, such as syndecan-1 or endocan,

✉ Takashi Takaki  
takaki@med.showa-u.ac.jp

<sup>1</sup> Department of Perioperative Medicine, Division of Anesthesiology, Showa University School of Dentistry, Tokyo, Japan  
<sup>2</sup> Center of Electron Microscopy, Showa University School, 1-5-8 Hatanodai, Shinagawa-Ku, Tokyo 142-8555, Japan  
<sup>3</sup> Department of Environmental Health, National Institute of Public Health, Saitama, Japan  
<sup>4</sup> Department of Anatomy, Showa University School of Medicine, Tokyo, Japan

could be quantitatively measured to evaluate GCX damage [6] in patients with pulmonary distress, including COVID-19 patients [7]. Since the GCX is a very thin and fragile layer, the fixation of GCX-containing specimens needs to be carefully considered to ensure the preservation of the natural architecture. Furthermore, pulmonary tissue itself is also fragile and can be difficult to fix in a manner that preserves its natural structure. Okada et al. obtained clear images of GCX structures in lung tissue using scanning electron microscopy (SEM) [8]. Their clear images were obtained using perfusion fixation, but this methodology cannot be applied to human specimens. Thus, the GCX remains difficult to visualize clinically. Our laboratory previously developed a methodology that enabled GCX visualization in mouse kidney specimens using formalin-fixed, epoxy resin-embedded ultra-thin sections [9]. This method enabled us to evaluate the GCX even in formalin-fixed specimens, which are often clinically available from patients. In the present study, we developed a method for visualizing lung GCX using immersion-fixed specimens.

## Methods

### Animals

Ten-week-old male BALB/c mice (Japan SLC Inc., Shizuoka, Japan) were used in this study.

This study was approved by the Animal Experiment Committee of Showa University (Animal experiment approval number #54025) and the Committee for Animal Experiments at the National Institute of Public Health (Protocol number R3-001). All animal experiments were conducted in accordance with the *Animal Research: Reporting of In Vivo Experiments* guidelines. Blood samples were collected from the heart under general anesthesia with a cocktail of 90 mg/kg of ketamine and 10 mg/kg of xylazine (FUJIFILM Wako Pure Chemicals Co. Osaka, Japan), after which the mice were euthanized and the lung specimens were collected.

### Development of optimal fixation method for GCX visualization in lung specimens

#### Investigation of the ALB immersion time and degassing frequency using optical microscopy

A solution consisting of 10% neutral buffered formalin (FUJIFILM Wako Pure Chemical, Osaka, Japan), 1% ALB 8GX (Sigma-Aldrich Japan, Tokyo, Japan), and 2% sucrose (FUJIFILM Wako Pure Chemicals Co. Osaka, Japan) was used as the ALB fixative (pH6.0) [9]. The mice were deeply anesthetized using the intramuscular injection of a ketamine and xylazine cocktail, then euthanized

via blood removal through a right atrial incision. A 5 mm square piece of mouse lung tissue was placed in a 10 mL syringe (TERUMO Tokyo, Japan) containing 5 mL of ALB fixative solution. Then, the syringe was capped (H4900C; Henke-Sass Wolf, Germany), and the syringe was pulled to 8 mL. The syringe was degassed 0, 30, 50, and 100 times at a speed of 1 pull/1 s. After degassing, the samples were immersed and fixed in ALB fixative at 4 °C for 1, 2, 3, 4, or 5 days. The samples were then embedded in ordinary paraffin; after cutting 1 mm from the tissue surface, sections with a thickness of 2 µm were prepared. After deparaffinization, the samples were observed using an optical microscope in an unsealed manner to examine the ALB dye penetration into the lung tissue. The findings were then compared according to the ALB immersion and fixation times as well as the degassing frequency, so as to determine the optimal values.

### Evaluation of tissue damage from degassing

To confirm the effect of degassing on the tissue specimens, two groups of TEM specimens were prepared: some lung tissue samples were fixed using the conventional method with lanthanum perfusion fixation (see Appendix), while others were fixed using 100 degassing repeats and 1 day of ALB immersion fixation. The samples were sectioned at 2 µm, stained with toluidine blue, and observed under an optical microscope. After ultra-thin sectioning (60 nm), the specimens were stained with 2% uranyl acetate and 2.7% lead citrate (Reynolds), then observed using TEM (H-7600; Hitachi High-Tech Co. Tokyo, Japan) at an acceleration voltage of 80 kV.

### Acquisition of SEM/TEM ultrastructural images of pulmonary vessels in specimens prepared using degassing and ALB immersion fixation

After degassing 0, 30, 50, or 100 times, the specimens were immersed in ALB fixation solution at 4 °C for 1 or 5 days, then treated with 10% neutral buffered formalin fixation for SEM (FlexSEM1000; Hitachi Tokyo, Japan)/TEM imaging. For the SEM specimens, lung tissues excised from mice were diced (5 mm); paraffin-embedded blocks were then sectioned at 2 µm. After deparaffinization and PAM staining, the specimens were air dried and observed without a metal coating using SEM and the backscattered electron mode at an acceleration voltage of 15 kV, a spot size of 40, and the low vacuum mode. For the TEM specimens, the lung tissues were sectioned into 1 mm squares, prepared using the conventional TEM procedure, and observed using TEM.

## Development of fast-track specimen preparation without paraffin embedding for SEM studies

Lung tissue excised from mice was diced (5 mm) and degassed 100 times. The specimens were then immersed in ALB fixative at 4 °C for 1 day and treated with 10% neutral buffered formalin fixation. The specimens were then dehydrated using a graded ethanol series. The samples were freeze-fractured, critical point-dried (931GL 8787A; TOUSIMIS Co., America), and osmium-coated (HPC-1SW osmium coater; VACUUM DEVICE Co., Japan), and then observed using SEM under the high vacuum mode.

## Confirmation of GCX visualization in pulmonary vessels using specimens from septic mice

### Septic mice

Lipopolysaccharide (LPS) (111: B4; Sigma-Aldrich Japan, Tokyo, Japan) was intraperitoneally administered at a dose of 8 mg/kg [10] to induce sepsis. A saline solution (same volume as that used for the septic model) was intraperitoneally administered for the control group. The survival rate was counted at 6, 12, and 24 h following LPS administration. A blood sample was collected from the heart under general anesthesia with ketamine, after which the mice were euthanized and lung specimens were collected. We confirmed the establishment of sepsis by measuring the body weight and the arterial blood pressure, O<sub>2</sub> saturation (SpO<sub>2</sub>), and serum mouse-soluble syndecan-1 (Sdc-1) level [measured using an enzyme-linked immunosorbent assay (ELISA); Diaclone SAS, Besancon Cedex, France]. The serum white blood cell (WBC) and platelet (PLT) counts were measured. SpO<sub>2</sub> was measured using MouseOx Plus (Starr Life Sciences Co., Oakmont, PA, USA) with a sensor attached to the thigh of each anesthetized mouse.

### Observation of endothelial GCX using SEM/TEM

Lung specimens were excised from septic mice for use in the SEM/TEM studies. The SEM specimens were prepared using a paraffin-unembedded technique. The samples were freeze-fractured, critical point-dried, and osmium-coated, and then observed using SEM under the high vacuum mode. The TEM specimens were prepared using a conventional procedure, then observed using TEM.

### Quantitative and area analyses of GCX in septic mice

The area and length of the GCX that was adhered to the pulmonary vascular endothelial surface in non-septic specimens prepared using lanthanum perfusion fixation, non-septic specimens prepared using a paraffin-unembedded technique,

and septic specimens prepared using a paraffin-unembedded technique were measured at 3 or 4 locations; the pixel areas were then calculated and compared using Adobe Photoshop Elements 2019.

The area of adhesion was calculated as the ratio of the number of pixels in the GCX area relative to the total number of pixels in the regions of interest, and the length of the adhesion was calculated as the ratio of the number of pixels occupied by the endothelial surface of the vessel immediately below the GCX relative to the total number of pixels occupied by the endothelial surface.

## Results

### Development of degassing and ALB immersion fixation technique

In all the specimens that had been degassed more than 30 times, the entire tissue was stained with ALB dye, regardless of the immersion time (1–5 days; Fig. 1). We concluded that 100 degassing repeats and 1 day of ALB immersion fixation were sufficient to yield optimal results. Therefore, 100 degassing repeats and 1 day of ALB immersion fixation were used for all subsequent experiments.

Optical microscopy confirmed that the morphology of the basement membrane was better preserved in specimens prepared with 100 degassing repeats and 1 day of ALB immersion, since toluidine blue-stained specimens prepared using perfusion fixation had dilated alveolar spaces and microvessels (Fig. 2a, b).

TEM observations showed a good morphological retention of erythrocytes and mitochondria in both specimens.

Observation of the lung microstructure revealed that the combination of 100 degassing repeats and ALB immersion fixation did not cause shrinkage or thinning of the basement membrane, epithelial cells, or endothelial cells, compared with perfusion fixation (Fig. 2c, d, e, f). Therefore, this method was judged to be suitable for fixing lung tissue.

### SEM/TEM ultrastructural imaging of pulmonary vessels in specimens prepared using degassing and ALB immersion fixation

The particle structure of the GCX was visible in specimens that had been degassed more than 30 times, and the GCX was diffusely scattered in SEM specimens that had been degassed 100 times (Fig. 3a, b, c, d, e). The GCX was clearly visible all around the endothelial surface in lung tissue specimens subjected to 100 degassing repeats and 1 day of ALB immersion fixation and observed using either SEM or TEM (Fig. 3f, g).

## duration of immersion

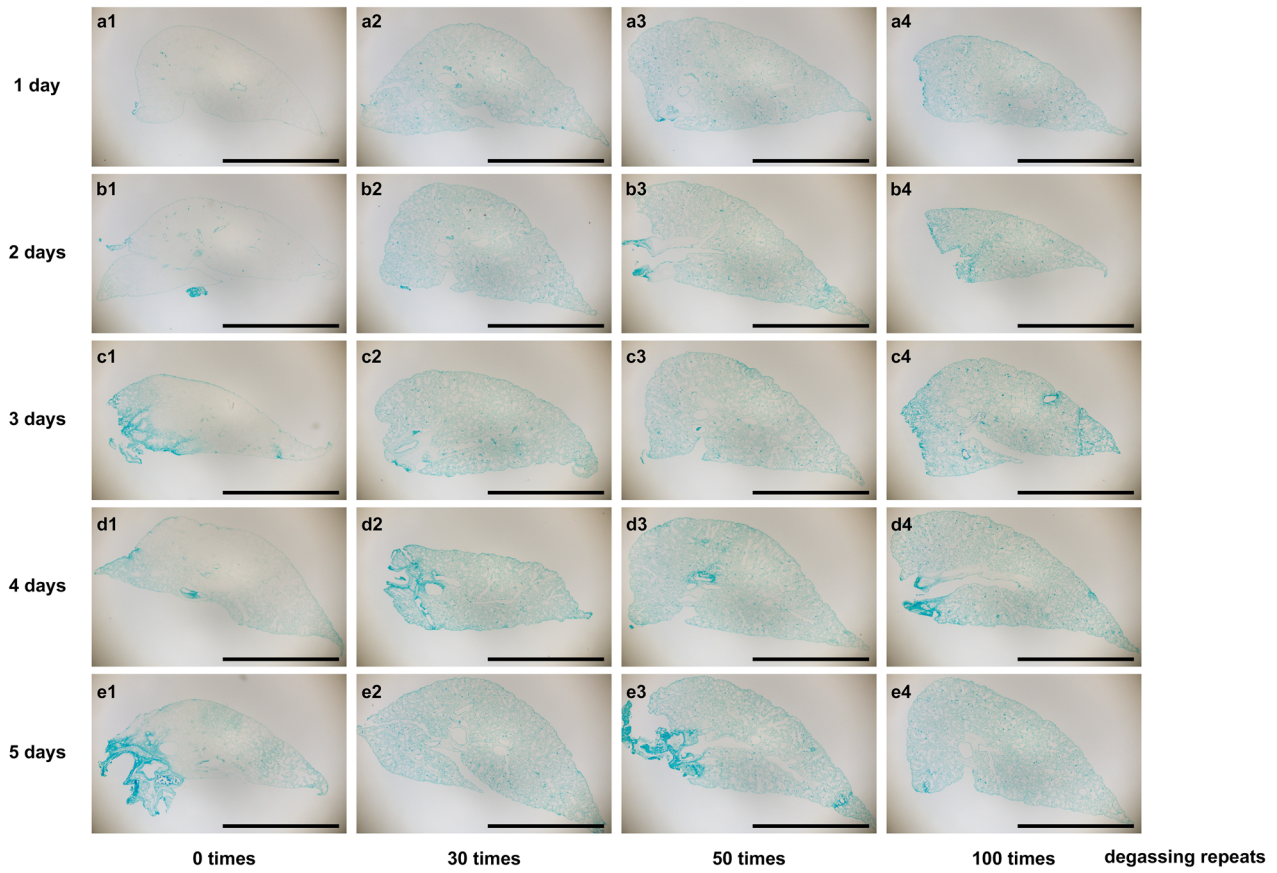


**Fig. 1** Effect of the frequency of degassing on the extent of fixation in the pulmonary tissue. The specimens were immersed in a solution composed of 10% neutral buffer formalin, 2% sucrose, and 1% Alcian blue (ALB) for 1–5 days after 0–100 degassing repeats to determine the optimal fixation conditions. Of note, the quality of staining after

100 degassing repeats and 1 day of fixation was almost identical to that after 100 degassing repeats and 5 days of fixation. We used these conditions for subsequent experiments. Magnification: **a–e**,  $\times 40$ . Scale bar: 2 mm

### Fast-track preparation of specimens without paraffin embedding for SEM

The GCX images obtained for specimens processed with FFPE preparation and PAM staining, which requires 6 days of processing, and for those processed with freeze-fractionation and osmium coating, which requires only 2 days of processing, were almost identical. Thus, the GCX was visible when the paraffin-unembedded technique, i.e., normal freeze-fractionation and osmium coating without FFPE specimen preparation and PAM staining, was used. Consequently, the processing time from lung tissue removal until SEM observation was shortened by 4 days. Furthermore, the morphology of the GCX in the specimens prepared using degassing and ALB immersion fixation was not obviously different from that in specimens prepared using lanthanum perfusion fixation (Fig. 4).

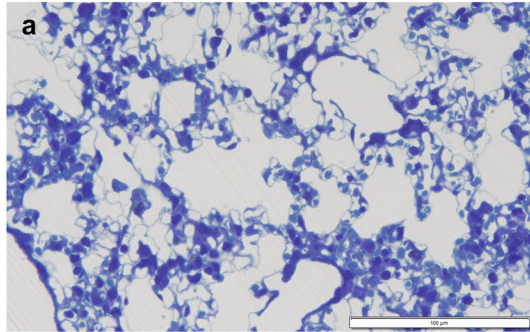
### Observation of GCX in pulmonary vessels in specimens from septic mice

#### Establishment of septic mouse model

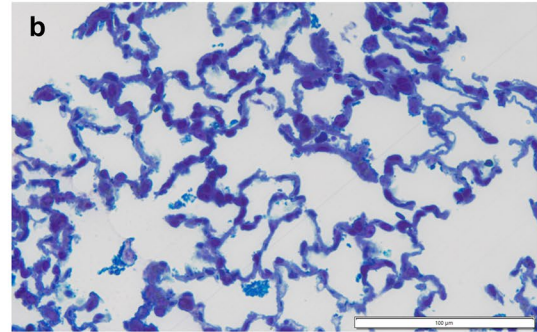
The largest WBC reduction was seen at 6 h after LPS administration, at which time the  $\text{SpO}_2$  had decreased from  $98.3 \pm 0.23\%$  before LPS administration to  $96.9\% \pm 0.47\%$  (Fig. 5A). The largest reductions in body weight, blood pressure, and blood PLT were observed at 12 h after LPS administration, at which time the  $\text{SpO}_2$  had decreased to  $93.3 \pm 1.55\%$  (Fig. 5B). The syndecan-1 level was highest at 12 h after administration. The survival rate was 100% at 12 h after LPS administration and 0% at 24 h after LPS administration (Fig. 5C). Therefore, the mice were used as a model of sepsis at 12 h after LPS administration.



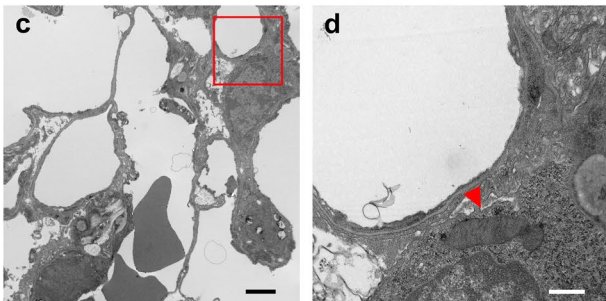
**Optical microscope:**  
perfusion fixation with lanthanum nitrate



**Optical microscope:**  
100 degassing repeats and 1 day ALB immersion fixation



**TEM: perfusion fixation with lanthanum nitrate**



**TEM: 100 degassing repeats and 1 day ALB immersion fixation**

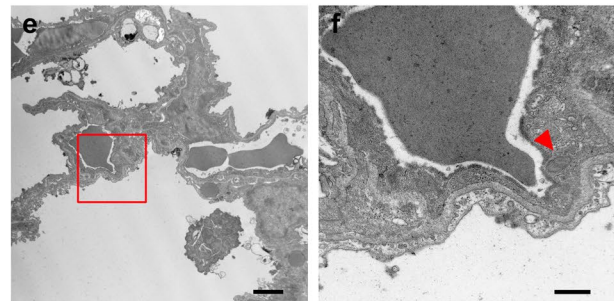


**Fig. 2** Confirmation of pulmonary specimen architecture after degassing. Tissue damage caused by degassing was evaluated by comparing images of specimens processed using perfusion fixation and specimens processed using 100 degassing repeats and 1 day of ALB immersion fixation. **a, c, d** Images of specimens processed using perfusion fixation. **b, e, f** Images of specimens processed using 100 degassing repeats and 1 day of ALB immersion fixation. **a, b** Optical microscopy images of lung tissue. The images of specimens pro-

cessed using perfusion fixation (**a**) or 100 degassing repeats and 1 day of ALB immersion fixation (**b**) were almost identical, with no artificial distortion of the architecture. **c, d, e, f** TEM images of lung tissue. The arrows indicate mitochondria. ALB immersion fixation did not cause shrinkage of the basement membrane, epithelial cells, or endothelial cells, compared with perfusion fixation. Magnifications: **a, b**,  $\times 400$ ; **c, e**,  $\times 2,500$ ; **d, f**,  $\times 12,000$ . Scale bar: **a, b**, 100  $\mu\text{m}$ ; **c, e**, 2  $\mu\text{m}$ ; **d, f**, 500 nm

### SEM images of the GCX in specimens from septic mice

The GCX was scattered as spherical aggregates across the surface of the pulmonary vascular endothelium in septic mice, while it covered the entire surface of the pulmonary vascular endothelium in non-septic mice (Fig. 5a). The mean area of adhered GCX on the pulmonary vascular endothelial surface ( $5 \times 8 \mu\text{m}$ ) corresponded to  $92.55 \pm 4.01\%$  of the endothelial surface in non-septic specimens prepared using perfusion fixation and  $93.77 \pm 2.71\%$  of the endothelial surface in non-septic specimens prepared using immersion fixation. Meanwhile, the mean area of adhered GCX in the septic specimens corresponded to  $34.67 \pm 14.63\%$  of the endothelial surface; this value was significantly lower ( $p < 0.05$ ) than that observed in non-septic mice (Fig. 6A).

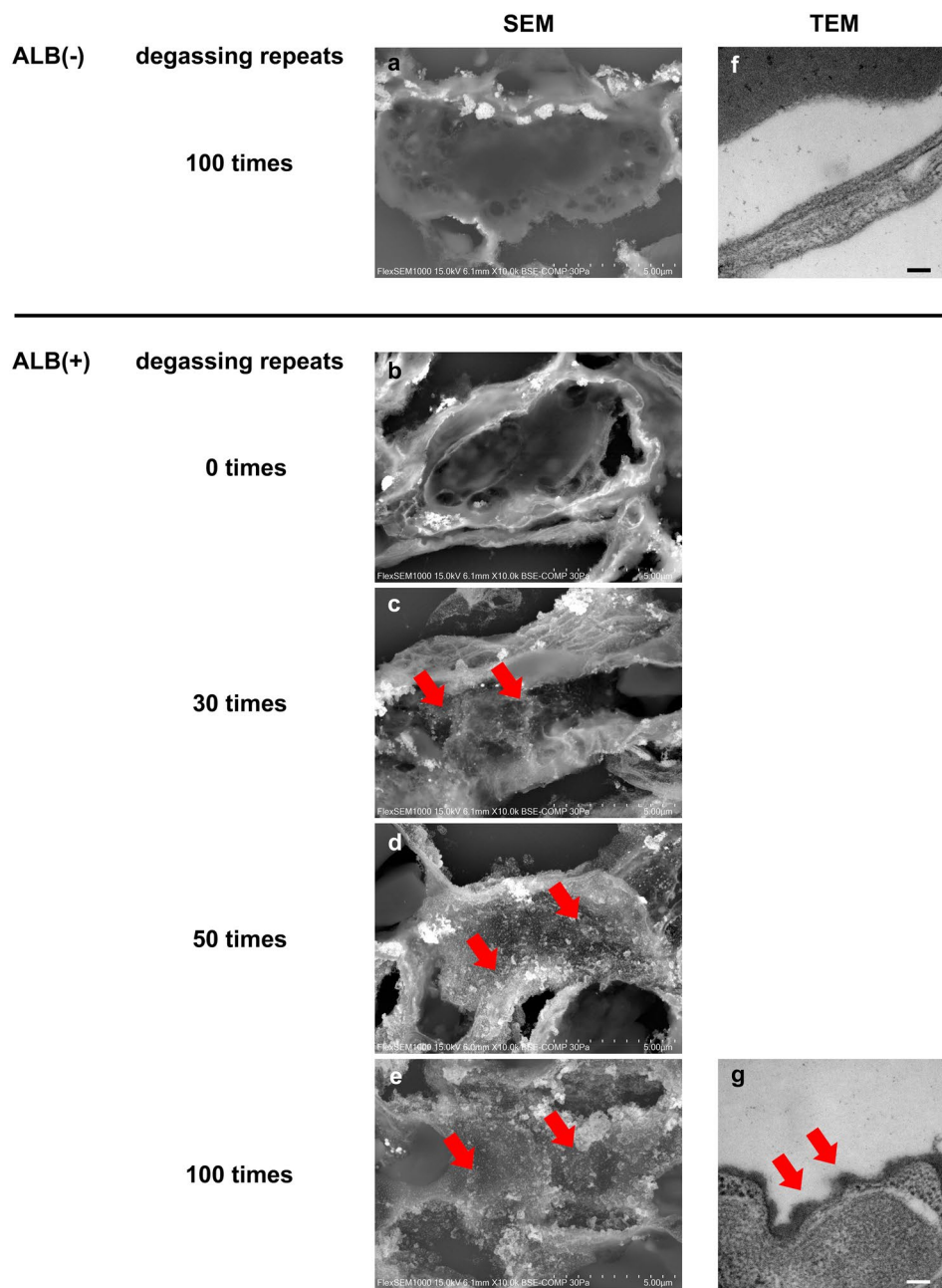
### TEM images of the GCX in specimens from septic mice

The TEM images confirmed that the GCX covered the pulmonary vascular endothelium nearly completely in

the non-septic specimens, while it was scattered in aggregates in the septic specimens (Fig. 5b). TEM observations showed that the GCX covered the entire surface of the pulmonary vascular endothelium in a partially hemispherical state in specimens from non-septic mice. In specimens from septic mice, however, the GCX did not cover the entire pulmonary vascular endothelial surface and was observed in a partially spherical, aggregated state.

The mean length of adhered GCX on the pulmonary vascular endothelial surface ( $200 \times 300 \text{ nm}$ ) corresponded to  $96.54 \pm 1.30\%$  of the length of the endothelial surface in non-septic specimens prepared using perfusion fixation and  $98.41 \pm 1.12\%$  of the length of the endothelial surface in non-septic specimens prepared using immersion fixation. Meanwhile, the length of adhered GCX in specimens from septic mice corresponded to  $43.65 \pm 8.26\%$  of the length of the endothelial surface; these values for non-septic and septic mice were significantly different ( $p < 0.05$ ) (Fig. 6B).

**Fig. 3** SEM and TEM images of pulmonary specimens processed using different degassing frequencies. The GCX was visible in the SEM and TEM images of specimens processed using ALB immersion fixation. Visualization of the components covering the pulmonary capillaries was confirmed for specimens processed using different degassing frequencies. More than 30 degassing repeats were required for the visualization of the GCX. Endothelial GCX imaging of the pulmonary capillaries was performed using ALB immersion with silver enhancement by PAM staining and was observed using LV-SEM (low vacuum SEM). **a, b, c, d, e** SEM images of lung tissue. **f, g** TEM images of lung tissue. **a, f** Pulmonary capillaries in specimens processed without ALB immersion fixation. The GCX cannot be observed on the surface of the vascular endothelium using either SEM or TEM. **b, c, d, e, g** Pulmonary capillaries in specimens processed using ALB immersion fixation for 1 day: (**b**) 0 degassing repeats, (**c**) 30 degassing repeats, (**d**) 50 degassing repeats, (**e, g**) 100 degassing repeats. The arrows indicate the endothelial glycocalyx. The GCX was clearly observed in specimens processed using 100 degassing repeats. Magnifications: **a, b, c, d, e**,  $\times 10,000$ ; **f, g**,  $\times 50,000$ . Scale bar: **a, b, c, d, e**, 5  $\mu\text{m}$ ; **f, g**, 100 nm



## Discussion

Our group previously succeeded in visualizing the renal GCX using ALB immersion-fixed specimens [9]. Here, we attempted to apply this method to the visualization of the GCX in lung tissue. Since lung tissue contains a considerable quantity of air, which interrupts the penetration of fixative, we used a degassing technique to overcome this problem. We confirmed that more than 100 degassing repeats were sufficient to allow the fixative solution to penetrate the tissue (Fig. 1). A syringe was used for the degassing and ALB immersion fixation; since subsequent electron

microscopy studies were capable of visualizing the GCX in these 100 degassing repeats and 1 day ALB immersion-fixed specimens, the effect of degassing on GCX observations was thought to be minimal.

We also confirmed that this procedure did not distort the ultrastructure of the lung tissue (Fig. 2). Previous studies have reported that the intratracheal instillation method is superior to other degassing or perfusion fixation methods for preserving lung tissue morphology for optical microscopy [11, 12]. These previous studies reported that the vacuum degassing method causes the expansion and thickening of alveolar walls; even using perfusion fixation, enlarged

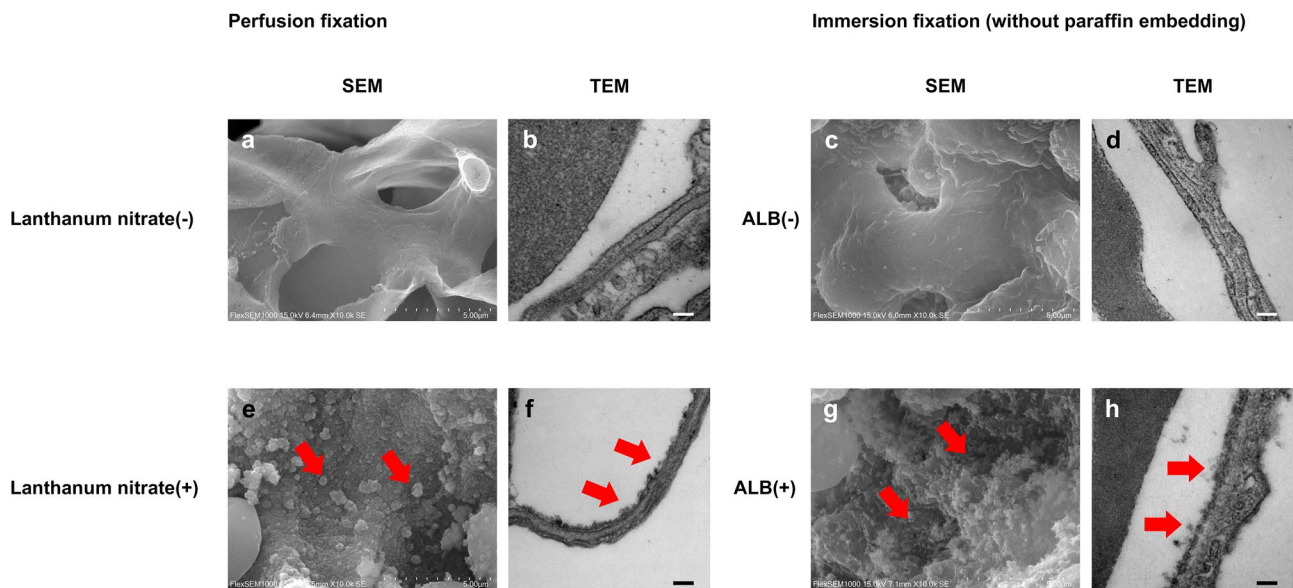


**Fig. 4** Comparison of SEM/TEM images for specimens processed using perfusion fixation and immersion fixation (without paraffin embedding). Of note, the SEM/TEM images were almost identical for specimens prepared using either process. The morphology of the GCX appears to be well preserved. **a, b, e, f** Images of specimens processed using perfusion fixation. **c, d, g, h** Images of specimens processed using immersion fixation (unembedded, with osmium coating). **a, c, e, g** SEM images of pulmonary capillaries. **b, d, f, h** TEM images of pulmonary capillaries. **a, b** Pulmonary capillaries in specimens processed without lanthanum nitrate. **c, d** Pulmonary capillaries

in specimens processed without ALB immersion. The GCX cannot be observed on the surface of the vascular endothelium using either SEM or TEM. **e, f** Pulmonary capillaries in specimens processed with lanthanum nitrate. **g, h** Pulmonary capillaries in specimens processed with ALB. The arrows indicate the GCX layer. No remarkable differences were noted between specimens processed using perfusion fixation and those processed using immersion fixation (without paraffin embedding). Magnifications: **a, c, e, g**,  $\times 10,000$ ; **b, d, f, h**,  $\times 50,000$ . Scale bar: **a, c, e, g**, 5  $\mu\text{m}$ ; **b, d, f, h**, 100 nm

alveoli, the collapse of lung parenchymal structures, and obvious hyper-cellularization and thickening of the alveolar walls can be observed. However, these previous reports were based on observations using optical microscopy, and GCX evaluations using electron microscopy were not performed. In the present study, TEM observations of the lung microstructure in specimens prepared using our degassing and ALB immersion method showed a good retention of the basement membrane and cells, and we determined that our method was suitable for TEM observations of the GCX in lung tissue specimens.

SEM images of the GCX in specimens prepared using 1 day of ALB immersion were almost identical to those prepared using 5 days of ALB immersion. Accordingly, we used 1 day of ALB immersion fixation in our subsequent analyses.

To simplify the preparation of SEM specimens for GCX observation even further, we applied osmium coating to the ALB immersion-fixed specimens. Using a process that does not require embedding, we were able to shorten the specimen processing time to approximately 2 days, which is 4 days shorter than the processing time required for PAM staining and paraffin embedding. We confirmed that the images obtained for specimens with osmium coating were comparable to those obtained for specimens prepared using

the conventional embedding technique. Our method may allow the depiction of the GCX via a reaction between ALB and osmium, suggesting that it might be possible to confirm the presence, amount, and adhesion of GCX in clinical pathological specimens using electron microscopy within a 24-h period, similar to techniques used for rapid pathological diagnosis.

Syndecan-1 and heparan sulfate, two biomarkers of GCX damage, reflect the degree of GCX loss from the vascular endothelial surface into the bloodstream, and these values have been reported to increase markedly during sepsis [2, 13]. Although these biomarkers are convenient for evaluating GCX damage, the marker levels are diluted by the entire circulating blood volume, and quantitative measurements are, thus, less sensitive than imaging analyses. The GCX layer on pulmonary vessels is also relatively thin, compared with that in other organs such as the heart and liver [14], and the contribution of GCX loss during pulmonary vascular injury to increases in the blood levels of syndecan-1 and heparin sulfate might be minimal.

Visualization of the GCX could also be applied to studies examining the pathophysiological mechanisms of cancer growth and therapeutic resistance in cancer or, alternatively, the development of pulmonary distress in



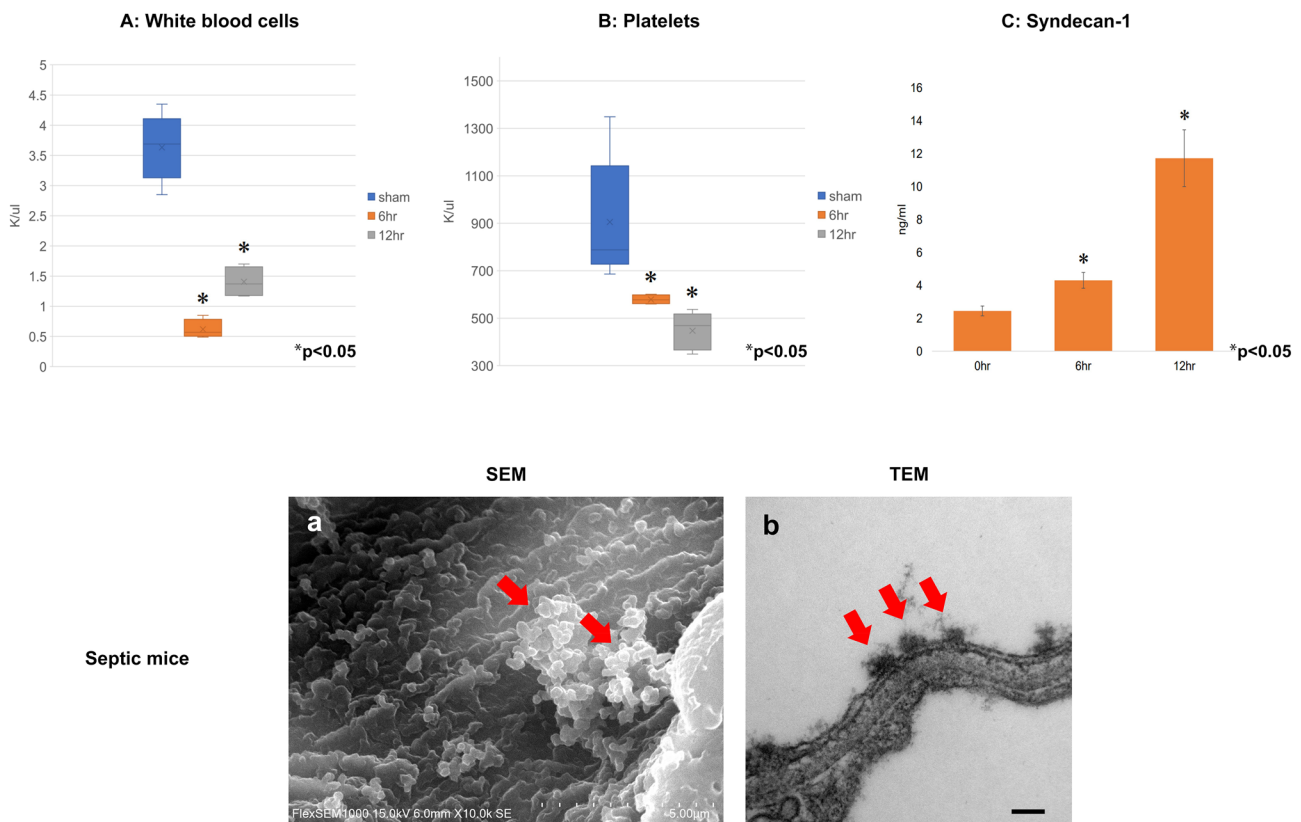


**Fig. 5** Establishment of septic mice and subsequent SEM/TEM images of the glycocalyx. The establishment of the septic mouse model was confirmed using specific biological parameters (white blood cells, platelets). The syndecan-1 level increased in parallel with the establishment of sepsis. **A** The white blood cell (WBC) count was significantly reduced at 6 and 12 h after LPS administration ( $p < 0.05$ ). **B** The platelet (PLT) count was significantly reduced at 6 and 12 h after LPS administration ( $p < 0.05$ ). **C** The syndecan-1 levels in blood samples obtained at 6 and 12 h after LPS administra-

tion were significantly increased ( $p < 0.05$ ). The presence of the GCX was confirmed in the septic mouse model. Of note, the GCX was less concentrated on the surface of the capillary lumen in both the TEM and SEM images. **a** SEM image of pulmonary capillaries from a septic mouse. The arrows indicate the glycocalyx layer. **b** TEM image of pulmonary capillaries from a septic mouse. The arrows indicate the glycocalyx layer. The GCX was scattered as spherical aggregates on the surface of the pulmonary vascular endothelium. Magnifications: **a**,  $\times 10,000$ ; **b**,  $\times 50,000$ . Scale bar: **a**, 5  $\mu\text{m}$ ; **b**, 100 nm

COVID-19. GCX is massively produced in metastatic cancers and is involved in cancer cell survival and growth [15, 16], contributing to the anti-cancer drug barrier on cell surfaces. Our research group previously showed that macrophages play an important role in the development of the lung edema that accompanies glycocalyx shedding [17]. We were able to confirm the role of macrophages in human lung injury by applying our newly developed method. Lung edema in patients with COVID-19 has also been shown to be accompanied by GCX depletion [18]. TEM observations of the ultrastructure of coronavirus particles, macrophages, and neutrophils in lung tissue have even been used to understand the pathogenesis of COVID-19 and to develop treatment strategies for COVID-19 [19]. The presently reported method might be applicable to diagnostic studies for cancer phenotype identification or to studies examining the pathogenesis of COVID-19, as well as the selection of effective anti-cancer drugs in clinical

practice and the selection of optimal clinical treatment strategies for cancer or COVID-19.

Finally, we confirmed the shedding of the GCX from the pulmonary vascular endothelium in septic mice, but we did not follow the process of GCX regeneration and recovery. Previous studies have shown that the GCX regenerates 48 h after GCX injury [13], but the mechanism of regeneration has not yet been clarified. Various therapeutical strategies have been assumed, and neutrophil elastase, thrombomodulin, and heparin are current candidates for the prevention of GCX shedding [20–26]. Our technique could help to evaluate the clinical efficacies of these medications in clinical practice.



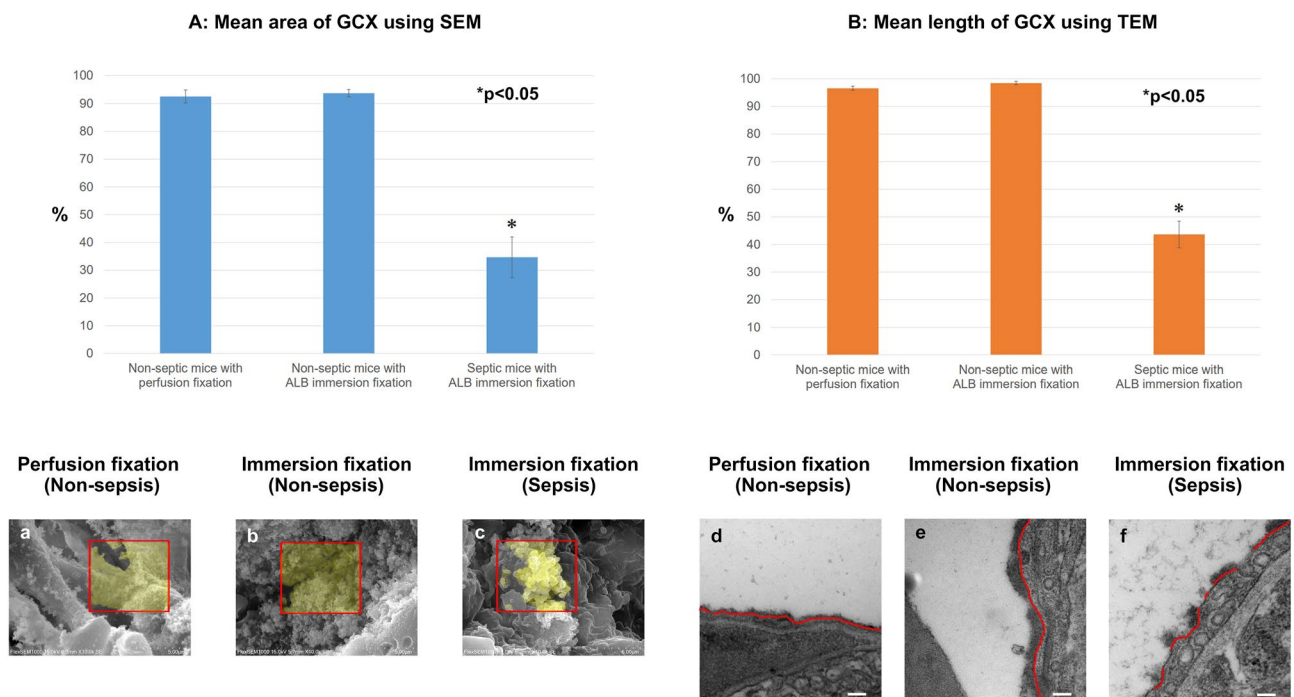


**Fig. 6** Quantitative and area analyses of GCX damage using SEM/TEM images. The density of the GCX was quantitatively evaluated using TEM and SEM images. **A** GCX density was measured as the GCX area ratio relative to the region of interest (ROI). **a** SEM image of a pulmonary capillary in a non-septic specimen processed using perfusion fixation. **b** SEM image of a pulmonary capillary in a non-septic specimen processed using ALB immersion fixation. **c** SEM image of a pulmonary capillary in a septic specimen processed using ALB immersion fixation. The GCX area ratio was measured within the red square in each group. The mean area of the GCX in the septic specimens was significantly smaller than that in the non-septic specimens processed using either perfusion or immersion fixation

( $p < 0.05$ ). **B** The GCX density was measured as the length of the luminal surface containing adhered GCX relative to the length of the ROI. **d** TEM image of a pulmonary capillary in a non-septic specimen processed using perfusion fixation. **e** TEM image of a pulmonary capillary in a non-septic specimen processed using ALB immersion fixation. **f** TEM image of a pulmonary capillary in a non-septic specimen processed using ALB immersion fixation. The length (red line) was measured in each group. The mean length of the GCX in specimens from septic mice was significantly smaller than that seen in non-septic specimens processed using perfusion or immersion fixation ( $p < 0.05$ ). Magnifications: **a, b, c**,  $\times 10,000$ ; **d, e, f**,  $\times 50,000$ . Scale bar: **a, b, c**, 5  $\mu\text{m}$ ; **d, e, f**, 100 nm

## Conclusion

This newly developed method of preparing specimens for GCX observation could be applied to not only animal lung tissue, but also human lung specimens. We expect that evaluations of morphological changes, from GCX shedding to regeneration, in humans will lead to the development of new treatment strategies for cancer or vascular permeability-enhanced pathologies, such as sepsis and ARDS, as well as research examining the function of the GCX itself.

## Appendix

### Conventional perfusion fixation with lanthanum nitrate

#### SEM

A solution consisting of 2.5% glutaraldehyde (Nisshin-EM Co. Tokyo, Japan), 2% sucrose, and 2% lanthanum nitrate (Sigma-Aldrich Japan, Tokyo, Japan) was used as the perfusion fixative.

The mice were deeply anesthetized using an intramuscular injection of a cocktail of ketamine and xylazine. A perfusion pump was used to perform the injection at a steady rate of 1 mL/min for about 15–20 min. The lungs were then harvested and diced into 5 mm cubes.

Each cube was immersed in the perfusion solution for one day of fixation at 4 °C. The specimens were then dehydrated using a graded ethanol series. Samples were freeze-cracked at the critical point, osmium-coated, and observed using SEM at an acceleration voltage of 15 kV, a spot size of 40, and the high vacuum mode [8, 27–30].

## TEM

Perfusion-fixed lungs were diced into 1-mm cubes and immersed in 2.5% glutaraldehyde, 2% sucrose, and 2% lanthanum nitrate fixing solution at 4 °C for one day. The specimens were then washed with 30 mM HEPES (DOJINDO LABORATORIES, Japan) and fixed in 2% osmium tetroxide at 4 °C for 2 h.

Specimens were dehydrated in a graded ethanol series and embedded in epoxy resin. After ultra-thin sectioning, the specimens were stained with 2% uranyl acetate and 2.7% lead citrate and were observed using TEM at an acceleration voltage of 80 kV [2, 9, 17].

**Acknowledgements** We thank Mr. Oniki and Ms. Nagai for their support with the specimen preparation at Showa University. We thank KAC Co. for preparing the paraffin-embedded blocks and slides. We thank Ms. Myrna Harrod-Taniguti for the English proofreading.

## Declarations

**Conflict of interest** The authors declare that they have no conflicts of interest.

## References

1. Ushiyama A, Kataoka H, Iijima T (2016) Glycocalyx and its involvement in clinical pathophysiology. *J Intensive Care* 4:59
2. Kataoka H, Ushiyama A, Akimoto Y, Matsubara S, Kawakami H, Iijima T (2017) Structural behavior of the endothelial glycocalyx is associated with pathophysiologic status in septic mice: an integrated approach to analyzing the behavior and function of the glycocalyx using both electron and fluorescence intravital microscopy. *Anesth Analg* 125:874–883
3. Becker BF, Chappell D, Brugger D, Annecke T, Jacob M (2010) Therapeutic strategies targeting the endothelial glycocalyx: acute deficits, but great potential. *Cardiovasc Res* 87:300–310
4. Chappell D, Brettner F, Doerfler N, Jacob M, Rehm M, Bruegger D, Conzen P, Jacob B, Becker BF (2014) Protection of glycocalyx decreases platelet adhesion after ischaemia/reperfusion: an animal study. *Eur J Anaesthesiol* 31:474–481
5. Shinohara A, Ushiyama A, Iijima T (2021) Time-dependent dynamics required for the degradation and restoration of the vascular endothelial glycocalyx layer in lipopolysaccharide-treated septic mice. *Front Cardiovasc Med* 8:730298
6. Fernandez-Sarmiento J, Molina CF, Salazar-Pelaez LM, Flórez S, Alarcón-Forero LC, Sarta M, Hernández-Sarmiento R, Villar JC (2022) Biomarkers of glycocalyx injury and endothelial activation are associated with clinical outcomes in patients with sepsis: a systematic review and meta-analysis. *J Intensive Care Med* 38:95–105
7. Astapenko D, Tomasova A, Ticha A, Hyspler R, Chua HS, Manzoor M, Skulec R, Lehmann C, Hahn RG, Malbrain ML, Cerny V (2022) Endothelial glycocalyx damage in patients with severe COVID-19 on mechanical ventilation—a prospective observational pilot study. *Clin Hemorheol Microcirc* 81:205–219
8. Okada H, Takemura G, Suzuki K, Oda K, Takada C, Hotta Y, Miyazaki N, Tsujimoto A, Muraki I, Ando Y, Zaikokuji R, Matsumoto A, Kitagaki H, Tamaoki Y, Usui T, Doi T, Yoshida T, Yoshida S, Ushikoshi H, Toyoda I, Ogura S (2017) Three-dimensional ultrastructure of capillary endothelial glycocalyx under normal and experimental endotoxemic conditions. *Crit Care* 21:261
9. Mukai S, Takaki T, Nagumo T, Sano M, Kang D, Takimoto M, Honda K (2021) Three-dimensional electron microscopy for endothelial glycocalyx observation using Alcian blue with silver enhancement. *Med Mol Morphol* 54:95–107
10. Thomas RC, Bath MF, Stover CM, Lambert DG, Thompson JP (2014) Exploring LPS-induced sepsis in rats and mice as a model to study potential protective effects of the nociceptin/orphanin FQ system. *Peptides* 61:56–60
11. Braber S, Verheijden KA, Henricks PA, Kraneveld AD, Folkerts G (2010) A comparison of fixation methods on lung morphology in a murine model of emphysema. *Am J Physiol Lung Cell Mol Physiol* 299:L843–851
12. Karasutani K, Baskoro H, Sato T, Arano N, Suzuki Y, Mitsui A, Shimada N, Kodama Y, Seyama K, Fukuchi Y, Takahashi K (2019) Lung fixation under constant pressure for evaluation of emphysema in mice. *J Vis Exp* 151:e58197
13. Inagawa R, Okada H, Takemura G, Suzuki K, Takada C, Yano H, Ando Y, Usui T, Hotta Y, Miyazaki N, Tsujimoto A, Zaikokuji R, Matsumoto A, Kawaguchi T, Doi T, Yoshida T, Yoshida S, Kumada K, Ushikoshi H, Toyoda I, Ogura S (2018) Ultrastructural alteration of pulmonary capillary endothelial glycocalyx during endotoxemia. *Chest* 154:317–325
14. Ando Y, Okada H, Takemura G, Suzuki K, Takada C, Tomita H, Zaikokuji R, Hotta Y, Miyazaki N, Yano H, Muraki I, Kuroda A, Fukuda H, Kawasaki Y, Okamoto H, Kawaguchi T, Watanabe T, Doi T, Yoshida T, Ushikoshi H, Yoshida S, Ogura S (2018) Brain-specific ultrastructure of capillary endothelial glycocalyx and its possible contribution for blood brain barrier. *Sci Rep* 8:17523
15. Tachi M, Okada H, Matsushashi N, Takemura G, Suzuki K, Fukuda H, Niwa A, Tanaka T, Mori H, Hara A, Yoshida K, Ogura S, Tomita H (2019) Human colorectal cancer infrastructure constructed by the glycocalyx. *J Clin Med* 8:1270
16. Paszek MJ, DuFort CC, Rossier O, Bainer R, Mouw JK, Godula K, Hudak JE, Lakins JN, Wijekoon AC, Cassereau L, Rubashkin MG, Magbanua MJ, Thorn KS, Davidson MW, Rugo HS, Park JW, Hammer DA, Giannone G, Bertozzi CR, Weaver VM (2014) The cancer glycocalyx mechanically primes integrin-mediated growth and survival. *Nature* 511:319–325
17. Nishida R, Suzuki D, Akimoto Y, Matsubara S, Hayakawa J, Ushiyama A, Sasa K, Miyamoto Y, Iijima T, Kamijo R (2023) Exploring the pathophysiological mechanism of interstitial edema focusing on the role of macrophages and their interaction with the glycocalyx. *J Oral Biosci* 65:111–118
18. Yamaoka-Tojo M (2020) Vascular endothelial glycocalyx damage in COVID-19. *Int J Mol Sci* 21:9712
19. Cortese K, Holland G, Möller L, Gagliani MC, Barisione E, Ball L, Pelosi P, Grillo F, Mastracci L, Fiocca R, Laue M (2022) Ultrastructural examination of lung “cryobiopsies” from a series of fatal COVID-19 cases hardly revealed infected cells. *Virchows Arch* 480:967–977
20. Suzuki K, Okada H, Takemura G, Takada C, Tomita H, Yano H, Muraki I, Zaikokuji R, Kuroda A, Fukuda H, Nishio A, Takashima S, Suzuki A, Miyazaki N, Fukuta T, Yamada N, Watanabe T, Doi T, Yoshida T, Kumada K, Ushikoshi H, Yoshida S, Ogura S (2020) Recombinant thrombomodulin protects against LPS-induced acute

- respiratory distress syndrome via preservation of pulmonary endothelial glycocalyx. *Br J Pharmacol* 177:4021–4033
21. Yini S, Heng Z, Xin A, Xiaochun M (2015) Effect of unfractionated heparin on endothelial glycocalyx in a septic shock model. *Acta Anaesthesiol Scand* 59:160–169
  22. Yang Y, Haeger SM, Sufita MA, Zhang F, Dailey KL, Colbert JF, Ford JA, Picon MA, Stearman RS, Lin L, Liu X, Han X, Linhardt RJ, Schmidt EP (2017) Fibroblast growth factor signaling mediates pulmonary endothelial glycocalyx reconstitution. *Am J Respir Cell Mol Biol* 56:727–737
  23. Tang Y, Wang X, Li Z, He Z, Yang X, Cheng X, Peng Y, Xue Q, Bai Y, Zhang R, Zhao K, Liang F, Xiao X, Andersson U, Wang H, Billiar TR, Lu B (2021) Heparin prevents caspase-11-dependent septic lethality independent of anticoagulant properties. *Immunity* 54:454–467
  24. Iba T, Levy JH, Aihara K, Kadota K, Tanaka H, Sato K, Nagaoka I (2020) Newly developed recombinant antithrombin protects the endothelial glycocalyx in an endotoxin-induced rat model of sepsis. *Int J Mol Sci* 22:176
  25. Li X, Zhu J, Liu K, Hu Y, Huang K, Pan S (2020) Heparin ameliorates cerebral edema and improves outcomes following status epilepticus by protecting endothelial glycocalyx in mice. *Exp Neurol* 330:113320
  26. Wang L, Huang X, Kong G, Xu H, Li J, Hao D, Wang T, Han S, Han C, Sun Y, Liu X, Wang X (2016) Ulinastatin attenuates pulmonary endothelial glycocalyx damage and inhibits endothelial heparanase activity in LPS-induced ARDS. *Biochem Biophys Res Commun* 478:669–675
  27. Chevalier L, Selim J, Genty D, Baste JM, Piton N, Boukhalfa I, Hamzaoui M, Pareige P, Richard V (2017) Electron microscopy approach for the visualization of the epithelial and endothelial glycocalyx. *Morphologie* 101:55–63
  28. Van den Berg BM, Vink H, Spaan JA (2003) The endothelial glycocalyx protects against myocardial edema. *Circ Res* 92:592–594
  29. Chappell D, Jacob M, Paul O, Rehm M, Welsch U, Stoeckelhuber M, Conzen P, Becker BF (2009) The glycocalyx of the human umbilical vein endothelial cell: an impressive structure ex vivo but not in culture. *Circ Res* 104:1313–1317
  30. Yang CY, Huynh T, Johnson M, Gong H (2014) Endothelial glycocalyx layer in the aqueous outflow pathway of bovine and human eyes. *Exp Eye Res* 128:27–33

**Publisher's Note** Springer Nature remains neutral with regard to jurisdictional claims in published maps and institutional affiliations.

Springer Nature or its licensor (e.g. a society or other partner) holds exclusive rights to this article under a publishing agreement with the author(s) or other rightsholder(s); author self-archiving of the accepted manuscript version of this article is solely governed by the terms of such publishing agreement and applicable law.